

# Localization beyond Dirac and Weyl fermions

Adesh Singh and Gargee Sharma

*School of Physical Sciences, Indian Institute of Technology Mandi, Mandi 175005, India*

In condensed matter, limited symmetry constraints allow free fermionic excitations to exist beyond the conventional Weyl and Dirac electrons of high-energy physics. These excitations carry a higher pseudospin, providing a natural generalization to the Weyl fermion. How do electrons beyond the conventional Dirac and Weyl fermions localize under disorder? In this Letter, we solve the problem of localization of free fermionic excitations carrying an arbitrary pseudospin- $s$ . We derive exact analytical expressions for fermionic wavefunctions, scattering time, renormalized velocity, Cooperon, and the magnetoconductivity. We discover that the gapless Cooperon mode solely depends on the pseudospin even when Fermi surface is composed of multiple pockets, leading to weak localization (antilocalization) behavior for even (odd)  $s$ . Remarkably, we find the localization correction to scale exponentially with  $s$ , i.e., faster moving electrons are strongly susceptible to disorder effects. This opens up intriguing possibility for Anderson localization and many-body localization in these materials.

*Introduction:* Electrons in a periodic potential can lead to free-fermionic excitations that display striking quantum mechanical properties. A foremost example is graphene [1, 2], where the additional sublattice degree of freedom provided by the honeycomb lattice maps its low-energy theory to that of a relativistic spin  $s = 1/2$  massless Dirac electron. Since the discovery of graphene, advances in material science have made it possible to realize a wide variety of fermionic excitations in systems such as topological insulators [3–5], Van der Waal heterostructures [6], Weyl and Dirac semimetals [7], topological superconductors [8–10], and the much celebrated moiré heterostructures [11–14]. These can display a wide variety of fascinating electronic properties, such as mimicking the high-energy Weyl, Dirac and Majorana fermions [5–10], hosting flat bands that can facilitate correlated physics [11–14], exhibiting higher pseudospin values [15], to name a few. The prospect of realizing these features in cold atomic lattices is a contemporary research theme [16, 17].

In high-energy physics, the constraints imposed by Poincaré symmetry makes it impossible to realize fermions beyond  $s = 1/2$ , but in condensed matter systems the constraints are lesser. Bradyln et al. [15] realized the possibility of finding free fermionic topological excitations in condensed matter systems that have no analogues in high-energy physics. These excitations, which are stabilized by certain symmetries, carry higher-pseudospins ( $s > 1/2$ ), are  $n$ -fold degenerate ( $n > 2$ ), and carry a nontrivial Chern number  $|C| > 1$  [15, 18–21]. Furthermore,  $\mathbf{k} \cdot \mathbf{p}$  theory and a corresponding low-energy  $\mathbf{k} \cdot \mathbf{S}$  Hamiltonian exists for systems belonging to certain spacegroups [15, 18].

Deviation from periodicity due to disorder is experimentally inevitable. Although disorder is typically not desirable, it can lead to intriguing phenomena of solely quantum origin. In the presence of strong disorder, electrons can localize leading to an Anderson insulating phase [22]. Constructive wave interference in even weakly

disordered solids leads to negative quantum correction to the Drude conductivity, known as weak localization (WL) [23–27], which is a precursor to Anderson localization. Interestingly in graphene, the pseudospin generates a Berry phase that leads to a destructive wave interference, resulting in a positive quantum correction to the conductivity [28–31]. This phenomena, known as weak antilocalization (WAL), was originally proposed to occur in a spin-orbit coupled two dimensional electron gas [28], where the rotation of the physical spin causes the phase difference. Despite intensive studies on localization of Dirac and Weyl fermions [29–40], the fate of free fermionic excitations beyond the Dirac and Weyl cases under disorder remains a highly pertinent unsolved question.

In this Letter, we solve the problem of quantum interference in fermions with arbitrary pseudospin ( $s$ ) dispersing linearly with momentum ( $\epsilon_{\mathbf{k}}^{ss'} \sim s'k$ ), where  $s$  can be either a positive integer or half integer, and  $-s \leq s' \leq s$ , increasing in steps of unity. We derive exact analytical expressions for the fermionic wavefunctions, elastic scattering time, renormalized semiclassical velocity, Cooperon, and the magnetoconductivity. We evaluate the Cooperon gaps and demonstrate that weak antilocalization occurs for half-integer pseudospins, while weak localization occurs for integer pseudospins. Remarkably, we find that the gapless Cooperon mode resulting in (anti)localization behavior depends only on the pseudospin, even when multiple bands cross the Fermi energy (for  $s \geq 3/2$ ). Therefore, if the Fermi surface consists of multiple pockets, localization corrections from all such bands is qualitatively similar. We discover weak localization (antilocalization) behavior for even (odd) pseudospin ( $s$ ), irrespective of the band index  $s'$ . For flat bands, we find zero quantum correction to conductivity. Remarkably, our analysis demonstrates that the localization correction scales exponentially with  $s$ , i.e., faster moving electrons are strongly susceptible to disorder effects. This insight suggests that the likelihood of encoun-

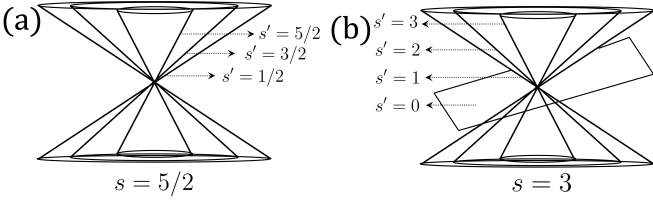


Figure 1. Energy dispersion of pseudospin- $s$  fermions plotted for two specific cases:  $s = 5/2$  and  $s = 3$ .

tering phenomena like Anderson localization and many-body localization is significantly increased. Our work not only generalizes the past work done in the context of Weyl and Dirac fermions [29–40] but provides crucial insights to the behavior of disordered electrons, paving way for novel explorations in the electronic properties of advanced materials.

*Model and formalism:* Pauli spin- $1/2$  matrices are generalized to the following matrices that describe fermions with pseudospin  $s$ :

$$\begin{aligned} (S_x)_{\alpha\beta} &= \frac{1}{2} (\delta_{\alpha,\beta+1} + \delta_{\alpha+1,\beta}) \sqrt{(s+1)(\alpha+\beta-1) - \alpha\beta} \\ (S_y)_{\alpha\beta} &= \frac{i}{2} (\delta_{\alpha,\beta+1} - \delta_{\alpha+1,\beta}) \sqrt{(s+1)(\alpha+\beta-1) - \alpha\beta} \\ (S_z)_{\alpha\beta} &= (s+1-\alpha)\delta_{\alpha,\beta} = (s+1-\beta)\delta_{\alpha,\beta} \end{aligned} \quad (1)$$

where  $1 \leq \alpha \leq 2s+1$ ,  $1 \leq \beta \leq 2s+1$ , and the pseudospin  $s \in \mathbb{Z}^+/2$ . We consider a low-energy  $k$ -space Hamiltonian of the type:

$$H_{\mathbf{k}}^s = \hbar v \mathbf{S} \cdot \mathbf{k}, \quad (2)$$

where  $v$  is a parameter that has dimensions of velocity, and  $\mathbf{k} = (k_x, k_y)$ , thus restricting ourselves to only two dimensions, although three-dimensional fermions are anticipated to exhibit qualitatively similar behavior [40]. This Hamiltonian generalizes the massless Weyl Hamiltonian and provides the low-energy theory for pseudospin- $s$  fermions with arbitrary pseudospin. Candidate materials for  $s = 1$  and  $s = 3/2$  are presented in Ref. [15]. The Hamiltonian has  $2s+1$  eigenvalues:  $\epsilon_{\mathbf{k}}/(\hbar v) = \{ks, k(s-1), k(s-2), \dots, -ks\}$ . When  $s$  is an integer, we obtain a dispersionless flat band ( $\epsilon_{\mathbf{k}} = 0$ ), which is absent for half-integer pseudospin (Fig. 1). Without any loss of generality, we assume the Fermi energy to have a finite positive value (electron doping).

When  $s \geq 3/2$ , multiple bands cross the Fermi energy, and we need to consider the combined effect from all such bands. Therefore, we denote the energy dispersion of the bands by  $\epsilon_{\mathbf{k}}^{ss'} = \hbar v s' k$ , where the first label in the superscript ( $ss'$ ) indicates the fermion pseudospin  $s$ , and the second label indicates the particular band with dispersion  $\hbar v s' k$ . The eigenfunctions corresponding to

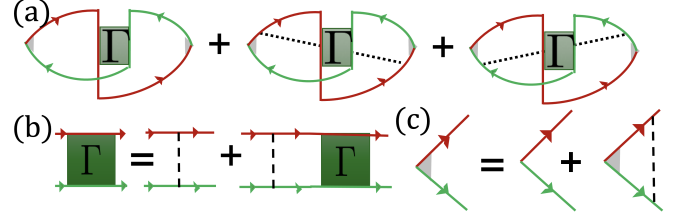


Figure 2. (a) Leading order Feynman diagrams for quantum interference correction to conductivity—bare and two dressed Hikami boxes. (b) Bethe-Salpeter equation for the Cooperon  $\Gamma$ . (c) Vertex correction to the velocity. The solid and dashed lines represent Green's functions and impurity scattering, respectively

$\epsilon_{\mathbf{k}}^{ss'}$  take the following form

$$|\mathbf{k}ss'\rangle = \mathcal{N}_{ss'} \sum_{m=0}^{2s} f_m^{ss'} e^{-im\phi}, \quad (3)$$

where  $\tan \phi = k_y/k_x$ ,  $f_m^{ss'}$  are the coefficients, and  $\mathcal{N}_{ss'}$  is the normalization constant. The analytical expressions for  $f_m^{ss'}$  are provided in [41]. Notably, we discover that the coefficients  $f_m^{ss'}$  have the structure of the Pascal's triangle [41].

We consider  $\delta$ -correlated scalar non-magnetic impurities given by the impurity potential  $U_0(\mathbf{r}) = \sum_i u_0 \mathbb{I}_{2s+1 \times 2s+1} \delta(\mathbf{r} - \mathbf{R}_i)$ , where the sum is over all impurity sites and  $u_0$  is average the impurity strength. The scattering (Born) amplitude is  $U_{\mathbf{k}\mathbf{k}'}^{ss'} = \langle \mathbf{k}ss' | U_0(\mathbf{r}) | \mathbf{k}'ss' \rangle$ , and the impurity average assumes the form  $\langle U_{\mathbf{k}\mathbf{k}'}^{ss'} U_{\mathbf{k}'\mathbf{k}}^{ss'} \rangle_{\text{imp}} = nu_0^2 \mathcal{F}^{ss'}(\phi - \phi')$ . The scattering time calculated via the Fermi's Golden rule is

$$\frac{1}{\tau_{ss'}} = \frac{2\pi}{\hbar} N_F^{s'} \mathcal{G}_{ss'} n_0 u_0^2, \quad (4)$$

where  $N_F^{s'} = E_F/2\pi(s'\hbar v)^2$  is the density of states at the Fermi energy. The coefficients  $\mathcal{G}_{ss'}$  and the functional form of  $\mathcal{F}^{ss'}(\phi)$  are specified in [41].

We next evaluate the ladder diagram correction to the quasiclassical velocity. The corresponding equation is given by (Fig. 2 (c))

$$\tilde{\mathbf{v}}_{\mathbf{k}}^{ss'} = \mathbf{v}_{\mathbf{k}}^{ss'} + \sum_{\mathbf{k}'} G_{\mathbf{k}'}^{ss'R} G_{\mathbf{k}'}^{ss'A} \langle U_{\mathbf{k}\mathbf{k}'}^{ss'} U_{\mathbf{k}'\mathbf{k}}^{ss'} \rangle_{\text{imp}} \tilde{\mathbf{v}}_{\mathbf{k}'}^{ss'}, \quad (5)$$

where  $\tilde{\mathbf{v}}_{\mathbf{k}}^{ss'}$  and  $\mathbf{v}_{\mathbf{k}}^{ss'}$  denote the impurity-dressed and bare velocity, respectively.  $G_{\mathbf{k}'}^{ss'R}$  and  $G_{\mathbf{k}'}^{ss'A}$  are retarded and advanced Green's functions, respectively, and are given by

$$G_{\mathbf{k}}^{ss'R/A}(\omega) = \frac{1}{\omega - \epsilon_{\mathbf{k}}^{ss'} \pm \frac{i\hbar}{2\tau_{ss'}}} \quad (6)$$

The ansatz  $\tilde{\mathbf{v}}_{\mathbf{k}}^{ss'} = \eta^{ss'} \mathbf{v}_{\mathbf{k}}^{ss'}$  solves Eq. 5, and  $\eta^{ss'}$  is eval-

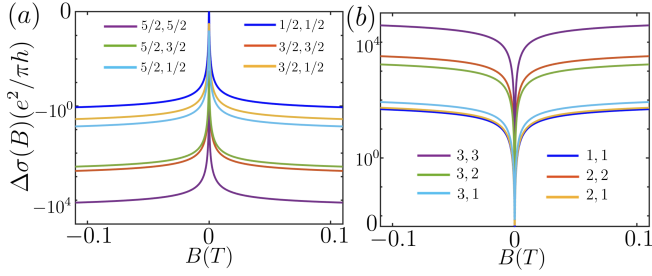


Figure 3. Magnetoelectricity of pseudospin- $s$  fermions. (a) WAL behavior for odd  $s$ . (b) WL behavior for even  $s$ . The exponential increase in magnitude with  $s'$  is striking. We choose  $l_\phi=300$  nm. Legends indicate  $\{s, s'\}$ .

uated in [41]. The quantum interference correction to conductivity, obtained by summing the contribution of a bare Hikami box ( $\sigma_0^F$ ) and two dressed Hikami boxes ( $\sigma_A^F$  and  $\sigma_A^R$ , (Fig. 2 (a))), are [41]

$$\begin{aligned} \sigma_0^F &= -\frac{e^2 s'^2 \vartheta^2 N_F^{s'} \eta_{ss'}^2 \tau_{ss'}^3}{\hbar^2} \sum_{\mathbf{q}} \Gamma(\mathbf{q}); & \sigma_A^R &= \sigma_A^F; \\ \sigma_A^F &= \frac{e^2 N_F^{s'} \tau_{ss'}^3 \eta_{ss'}^2 \vartheta^2 s'^2}{4\hbar^2 \mathcal{G}_{ss'}} \mathcal{A}_1^{ss'} \sum_{\mathbf{q}} \Gamma(\mathbf{q}), \end{aligned} \quad (7)$$

where  $\Gamma(\mathbf{q})$  is the vertex ((Fig. 2 (b))), and  $\mathcal{A}_m^{ss'}$  are the coefficients of the bare vertex, defined in Eq. 9. As a sanity check, we recover the results for graphene:  $\eta^{\frac{1}{2}} = 2$ ,  $\mathcal{F}^{\frac{1}{2}}(\phi) = \cos^2(\phi/2)$ ,  $\sigma_A^F/\sigma_0^F = -1/4$  [29–31]. The Bethe-Salpeter equation for the vertex is given by

$$\Gamma_{\mathbf{k}_1, \mathbf{k}_2}^{ss'} = \Gamma_{\mathbf{k}_1, \mathbf{k}_2}^{ss'0} + \sum_{\mathbf{k}} \Gamma_{\mathbf{k}_1, \mathbf{k}}^{ss'0} G_{\mathbf{k}}^{ss'R} G_{\mathbf{q}-\mathbf{k}}^{ss'A} \Gamma_{\mathbf{k}, \mathbf{k}_2}^{ss'}, \quad (8)$$

where the bare vertex  $\Gamma_{\mathbf{k}_1, \mathbf{k}_2}^{ss'0} = \langle U_{\mathbf{k}_1 \mathbf{k}_2}^{ss'} U_{-\mathbf{k}_1 \mathbf{k}_2}^{ss'} \rangle_{\text{imp}}$  is evaluated to take the following form :

$$\Gamma_{\mathbf{k}_1, \mathbf{k}_2}^{ss'0} = \left( \frac{\hbar}{2\pi N_F^{s'} \mathcal{G}_{ss'} \tau_{ss'}} \right) \sum_{m=0}^{4s} \mathcal{A}_m^{ss'} e^{im(\phi_1 - \phi_2)}. \quad (9)$$

The evaluated coefficients  $\mathcal{A}_m^{ss'}$  are specified in [41]. We assume the following ansatz for the dressed vertex:

$$\Gamma_{\mathbf{k}_1, \mathbf{k}_2}^{ss'} = \left( \frac{\hbar}{2\pi N_F^{s'} \mathcal{G}_{ss'} \tau_{ss'}} \right) \sum_{m=0}^{4s} \sum_{n=0}^{4s} \mathcal{V}_{mn}^{ss'} e^{i(m\phi_1 - n\phi_2)}, \quad (10)$$

which solves the Bethe-Salpeter equation Eq. 8. The coefficients of the matrix  $\mathcal{V}^{ss'}$  are given by the solution of the following equation:

$$\mathcal{V}^{ss'} = (1 - \mathcal{A}^{ss'} \Phi^{ss'} \mathcal{G}_{ss'}^{-1})^{-1} \mathcal{A}^{ss'}, \quad (11)$$

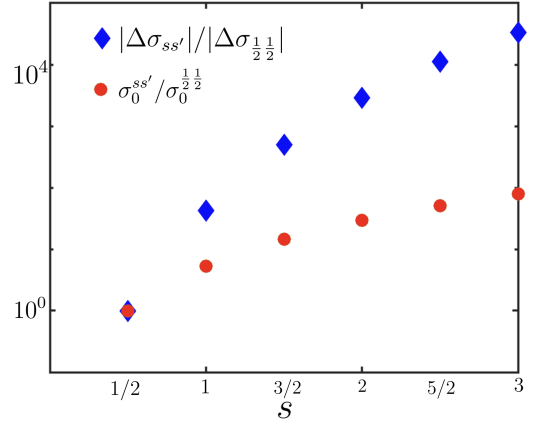


Figure 4. The relative increase of localization induced magnetoelectricity (blue) and the Drude conductivity (red) for pseudospin- $s$  fermions. We choose  $s' = s$ .

where [41]

$$\begin{aligned} \Phi_{mn}^{ss'} &= \int \frac{d\phi}{2\pi} \frac{e^{i(n-m)\phi}}{1 + i\tau_{ss'} \vartheta s' q \cos \phi} \\ &= \left(1 - \frac{Q^2}{2}\right) \delta_{mn} - \frac{iQ}{2} (\delta_{m, n+1} + \delta_{m, n-1}) \\ &\quad - \frac{Q^2}{4} (\delta_{m, n+2} + \delta_{m, n-2}), \end{aligned} \quad (12)$$

and  $Q = \vartheta \tau_{ss'} s' q$ . The diverging elements of  $\mathcal{V}^{ss'}$  give us information about the vanishing Cooperon gaps that result in localization behavior.

*Conductivity:* The zero-field quantum interference correction to the conductivity from the gapless Cooperon mode  $\alpha$  for the band  $|\mathbf{k}ss'\rangle$  is evaluated to be

$$\sigma_{ss'} = -\frac{e^2}{2\pi\hbar} Y_\alpha^{ss'} \ln(l_\phi/l_{ss'}) e^{i\alpha\pi}, \quad (13)$$

where  $l_\phi$  is the coherence length, and

$$\begin{aligned} Y_\alpha^{ss'} &= \frac{\eta^{ss'2} s'^2}{4X_\alpha^{ss'} \mathcal{G}_{ss'}^2} \left(1 - \frac{\mathcal{A}_1^{ss'}}{2\mathcal{G}_{ss'}}\right), \\ l_{ss'}^{-2} &= \frac{2}{\vartheta^2 \tau_{ss'}^2}, \quad \mathcal{X}_\alpha^{ss'} = \frac{2}{\mathcal{V}_{\alpha\alpha}^{ss'} Q^2} \end{aligned} \quad (14)$$

Remarkably, we discover that the gapless Cooperon mode  $\alpha$  is independent of the band index  $s'$  and only depends on the pseudospin  $s$  [41]. Specifically, we find  $\alpha = 2s$ . Therefore, if multiple bands ( $|\mathbf{k}ss'\rangle$  and  $|\mathbf{k}ss''\rangle$ ) intersect the Fermi energy, localization corrections from all of them will be qualitatively similar. We discover that for odd (even) pseudospin,  $e^{i\alpha\pi} = -1$  ( $e^{i\alpha\pi} = +1$ ), resulting in weak antilocalization (localization) behavior. The exponential factor  $e^{i\alpha\pi}$  can also be identified with the Berry phase of the pseudospin, which lies at the core of localization-antilocalization behavior. In-

terestingly, it is the Berry phase of the pseudospin enters in the equation (Eq. 13) and not the Berry phase of the particular band, but since they are the identical ( $e^{2\pi i s} = e^{2\pi i s'}$  for a given pseudospin  $s$ , if  $s' \neq 0$ ) in this model, it does not lead to any difference. Note that even though the Berry phase contribution is independent of  $s'$ ,  $Y_\alpha^{ss'}$  depends on  $s'$ , and thus the conductivity corrections for  $|\mathbf{k}ss'\rangle$  and  $|\mathbf{k}ss''\rangle$  are quantitatively different. We also predict that for flat bands ( $s' = 0$ ), quantum corrections vanish. With application of a magnetic field, the phase coherence is lost and the quantum correction is suppressed. This enables the experimental observation of weak localization and weak antilocalization corrections through magnetoconductivity measurements. This can be derived by quantizing the wavevector  $q^2 \rightarrow (n+1/2)(4eB/\hbar^2)$ . In the weak-field limit, the magnetoconductivity ( $\Delta\sigma(B)_{ss'} = \sigma(B)_{ss'} - \sigma_{ss'}$ ) is given by

$$\Delta\sigma(B)_{ss'} = \frac{e^2}{\pi h} Y_\alpha^{ss'} \left[ \Psi \left( \frac{l_B^2}{l_\phi^2} + \frac{1}{2} \right) - \ln \left( \frac{l_B^2}{l_\phi^2} \right) \right] e^{i\alpha\pi}, \quad (15)$$

where  $\Psi(x)$  is the digamma function. Notably, the zero-field conductivity correction (Eq. 13) and the magnetoconductivity crucially depend on the same prefactor  $Y_\alpha^{ss'}$  that governs the magnitude of the correction. Eq. 13-15 are the main results of this paper that generalize all the existing results for the Dirac/Weyl fermion to arbitrary pseudospin- $s$ .

In Fig. 3 we plot the magnetoconductivity for both odd and even pseudospin- $s$  fermions limiting ourselves to  $s \leq 3$ , including all  $0 < s' \leq s$ . Both the WAL correction (for odd  $s$ ) and WL correction (for even  $s$ ) scale exponentially with increase in  $s'$ . On the other hand, magnetoconductivity for same  $s'$  but different  $s$  have comparable orders of magnitude (for example  $\{s, s'\} = \{1/2, 1/2\}$ ,  $\{3/2, 1/2\}$  and  $\{5/2, 1/2\}$  have a similar order of magnitude). Therefore the magnitude of the localization correction is strongly dependent on  $s'$  and not  $s$ , but since larger values of  $s'$  are only possible for larger values of  $s$ , higher pseudospins do lead to stronger localization correction. It can be argued then that for large  $s$ , perturbation theory may break down at comparatively lesser magnetic fields. Nevertheless, quantum effects will still lead to strong localization.

The Drude conductivity calculated for pseudospin- $s$ , yields a rather simple expression:

$$\sigma_0^{ss'} = \frac{e^2}{h} \left( \frac{\varphi^2 s'^2}{\mathcal{G}_{ss'} n_0 u_0^2} \right), \quad (16)$$

which scales approximately with the second power of  $s'$ . We further test our theory by comparing the relative increase of the Drude conductivity and the quantum interference correction. In Fig. 4 we plot the relative increase in magnetoconductivity  $|\Delta\sigma_{ss}|/|\Delta\sigma_{\frac{1}{2}}|$  and

the relative increase in the Drude conductivity  $\sigma_0^{ss}/\sigma_0^{\frac{1}{2}}$ . While  $\sigma_0 \sim s^2$ ,  $\Delta\sigma_{ss}$  scales up much more drastically.

*Interactions:* The interaction parameter  $r_s$  represents the ratio of the average inter-electron Coulomb interaction energy to the Fermi energy. The average Coulomb energy is  $\langle V \rangle \sim e^2/\langle r \rangle$ , where  $\langle r \rangle = n^{-1/2} \sim s'/k_F$  is the average inter-particle separation. Therefore,  $r_s \sim s'^{-1}$  indicating that electron-electron interactions are less dominant for higher pseudospins. However, as we discussed, strong localization induced by even weak or moderate disorder may interplay with interactions and lead to more surprising and exotic possibilities such as many body localization that may be explored in upcoming studies. Detailed study of electron-electron interactions for pseudospin- $s$  fermions is reserved for future works.

*Summary and Outlook:* Advances in material science have enabled the realization of a manifold of emergent electronic excitations, from massless Dirac and Weyl excitations to flat-bands in moiré materials. Combined with theoretical predictions of realizing materials that host higher pseudospin fermions in solids (at least up to  $s = 2$  [15]), these developments open up exciting possibilities for studying quantum transport such materials. We solved the fundamental problem of disorder induced quantum interference corrections leading to electron (anti)localization in fermionic excitations that carry an arbitrary pseudospin  $s$ . Deriving exact analytical expressions for the relevant quantities allows us to reveal that the gapless Cooperon modes depends exclusively on the pseudospin, resulting in in weak localization (antilocalization) behavior for even (odd)  $s$ . An astounding finding of our work is that the localization correction scales exponentially with  $s$ . We generalize existing works on localization effects in Weyl and Dirac fermions, and provide crucial insights that push forward our fundamental understanding of how disorder and interactions may interplay in these materials.

- 
- [1] A. C. Neto, F. Guinea, N. M. Peres, K. S. Novoselov, and A. K. Geim, The electronic properties of graphene, *Reviews of modern physics* **81**, 109 (2009).
  - [2] S. D. Sarma, S. Adam, E. Hwang, and E. Rossi, Electronic transport in two-dimensional graphene, *Reviews of modern physics* **83**, 407 (2011).
  - [3] M. Z. Hasan and C. L. Kane, Colloquium: topological insulators, *Reviews of modern physics* **82**, 3045 (2010).
  - [4] X.-L. Qi and S.-C. Zhang, Topological insulators and superconductors, *Reviews of modern physics* **83**, 1057 (2011).
  - [5] O. Vafek and A. Vishwanath, Dirac fermions in solids: from high- $T_c$  cuprates and graphene to topological insulators and weyl semimetals, *Annu. Rev. Condens. Matter Phys.* **5**, 83 (2014).
  - [6] A. K. Geim and I. V. Grigorieva, Van der waals heterostructures, *Nature* **499**, 419 (2013).

- [7] N. Armitage, E. Mele, and A. Vishwanath, Weyl and dirac semimetals in three-dimensional solids, *Reviews of Modern Physics* **90**, 015001 (2018).
- [8] A. Y. Kitaev, Unpaired majorana fermions in quantum wires, *Physics-Uspekhi* **44**, 131 (2001).
- [9] R. M. Lutchyn, J. D. Sau, and S. D. Sarma, Majorana fermions and a topological phase transition in semiconductor-superconductor heterostructures, *Physical review letters* **105**, 077001 (2010).
- [10] Y. Oreg, G. Refael, and F. von Oppen, Helical liquids and majorana bound states in quantum wires, *Physical review letters* **105**, 177002 (2010).
- [11] Y. Cao, V. Fatemi, S. Fang, K. Watanabe, T. Taniguchi, E. Kaxiras, and P. Jarillo-Herrero, Unconventional superconductivity in magic-angle graphene superlattices, *Nature* **556**, 43 (2018).
- [12] Y. Cao, V. Fatemi, A. Demir, S. Fang, S. L. Tomarken, J. Y. Luo, J. D. Sanchez-Yamagishi, K. Watanabe, T. Taniguchi, E. Kaxiras, *et al.*, Correlated insulator behaviour at half-filling in magic-angle graphene superlattices, *Nature* **556**, 80 (2018).
- [13] M. Yankowitz, S. Chen, H. Polshyn, Y. Zhang, K. Watanabe, T. Taniguchi, D. Graf, A. F. Young, and C. R. Dean, Tuning superconductivity in twisted bilayer graphene, *Science*, eaav1910 (2019).
- [14] E. Gibney, How ‘magic angle’ graphene is stirring up physics, *Nature* **565**, 15 (2019).
- [15] B. Bradlyn, J. Cano, Z. Wang, M. Vergniory, C. Felser, R. J. Cava, and B. A. Bernevig, Beyond dirac and weyl fermions: Unconventional quasiparticles in conventional crystals, *Science* **353**, aaf5037 (2016).
- [16] N. Goldman, J. C. Budich, and P. Zoller, Topological quantum matter with ultracold gases in optical lattices, *Nature Physics* **12**, 639 (2016).
- [17] D.-W. Zhang, Y.-Q. Zhu, Y. Zhao, H. Yan, and S.-L. Zhu, Topological quantum matter with cold atoms, *Advances in Physics* **67**, 253 (2018).
- [18] C. Bradley, *C racknell*, ap: The mathematical theory of symmetry in solids, clarendon (1972).
- [19] B. J. Wieder, Y. Kim, A. Rappe, and C. Kane, Double dirac semimetals in three dimensions, *Physical review letters* **116**, 186402 (2016).
- [20] A. Raoux, M. Morigi, J.-N. Fuchs, F. Piéchon, and G. Montambaux, From dia-to paramagnetic orbital susceptibility of massless fermions, *Physical Review Letters* **112**, 026402 (2014).
- [21] M. Ezawa, Pseudospin-3 2 fermions, type-ii weyl semimetals, and critical weyl semimetals in tricolor cubic lattices, *Physical Review B* **94**, 195205 (2016).
- [22] P. W. Anderson, Absence of diffusion in certain random lattices, *Physical review* **109**, 1492 (1958).
- [23] P. A. Lee and T. Ramakrishnan, Disordered electronic systems, *Reviews of modern physics* **57**, 287 (1985).
- [24] E. Akkermans and G. Montambaux, *Mesoscopic physics of electrons and photons* (Cambridge university press, 2007).
- [25] B. Altshuler, D. Khmel’Nitzkii, A. Larkin, and P. Lee, Magnetoresistance and hall effect in a disordered two-dimensional electron gas, *Physical Review B* **22**, 5142 (1980).
- [26] G. Bergmann, Weak localization in thin films: a time-of-flight experiment with conduction electrons, *Physics Reports* **107**, 1 (1984).
- [27] S. Chakravarty and A. Schmid, Weak localization: The quasiclassical theory of electrons in a random potential, *Physics Reports* **140**, 193 (1986).
- [28] S. Hikami, A. I. Larkin, and Y. Nagaoka, Spin-orbit interaction and magnetoresistance in the two dimensional random system, *Progress of Theoretical Physics* **63**, 707 (1980).
- [29] H. Suzuura and T. Ando, Crossover from symplectic to orthogonal class in a two-dimensional honeycomb lattice, *Physical Review Letters* **89**, 266603 (2002).
- [30] D. Khveshchenko, Electron localization properties in graphene, *Physical Review Letters* **97**, 036802 (2006).
- [31] E. McCann, K. Kechedzhi, V. I. Fal’ko, H. Suzuura, T. Ando, and B. Altshuler, Weak-localization magnetoresistance and valley symmetry in graphene, *Physical Review Letters* **97**, 146805 (2006).
- [32] R. Gorbachev, F. Tikhonenko, A. Mayorov, D. Horsell, and A. Savchenko, Weak localization in bilayer graphene, *Physical Review Letters* **98**, 176805 (2007).
- [33] X. Wu, X. Li, Z. Song, C. Berger, and W. A. de Heer, Weak antilocalization in epitaxial graphene: Evidence for chiral electrons, *Physical Review Letters* **98**, 136801 (2007).
- [34] F. Tikhonenko, D. Horsell, R. Gorbachev, and A. Savchenko, Weak localization in graphene flakes, *Physical Review Letters* **100**, 056802 (2008).
- [35] G. Tkachov and E. Hankiewicz, Weak antilocalization in hgte quantum wells and topological surface states: Massive versus massless dirac fermions, *Physical Review B* **84**, 035444 (2011).
- [36] A. Singh and G. Sharma, Quantum interference of pseudospin-1 fermions, *Physical Review B* **108**, 195426 (2023).
- [37] H.-Z. Lu, J. Shi, and S.-Q. Shen, Competition between weak localization and antilocalization in topological surface states, *Physical Review Letters* **107**, 076801 (2011).
- [38] H.-Z. Lu, W. Yao, D. Xiao, and S.-Q. Shen, Intervalley scattering and localization behaviors of spin-valley coupled dirac fermions, *Physical Review Letters* **110**, 016806 (2013).
- [39] H.-Z. Lu and S.-Q. Shen, Finite-temperature conductivity and magnetoconductivity of topological insulators, *Physical Review Letters* **112**, 146601 (2014).
- [40] B. Fu, H.-W. Wang, and S.-Q. Shen, Quantum interference theory of magnetoresistance in dirac materials, *Physical Review Letters* **122**, 246601 (2019).
- [41] A. Singh and G. Sharma, See supplementary information, (2024).

SUPPLEMENTAL MATERIAL TO ‘LOCALIZATION BEYOND DIRAC AND WEYL FERMIONS’

MODEL

Pseudospin- $s$  fermions

Pauli spin-1/2 matrices are generalized to the following matrices that describe fermions with pseudospin  $s$ :

$$\begin{aligned} (S_x)_{\alpha\beta} &= \frac{1}{2} (\delta_{\alpha,\beta+1} + \delta_{\alpha+1,\beta}) \sqrt{(s+1)(\alpha+\beta-1) - \alpha\beta} \\ (S_y)_{\alpha\beta} &= \frac{i}{2} (\delta_{\alpha,\beta+1} - \delta_{\alpha+1,\beta}) \sqrt{(s+1)(\alpha+\beta-1) - \alpha\beta} \\ (S_z)_{\alpha\beta} &= (s+1-\alpha)\delta_{\alpha,\beta} = (s+1-\beta)\delta_{\alpha,\beta} \end{aligned} \quad (17)$$

where  $1 \leq \alpha \leq 2s+1$ ,  $1 \leq \beta \leq 2s+1$ , and the pseudospin  $s \in \mathbb{Z}^+/2$ . We consider a low-energy  $k$ -space Hamiltonian of the type:

$$H_{\mathbf{k}}^s = \hbar\vartheta \mathbf{S} \cdot \mathbf{k}, \quad (18)$$

where  $\vartheta$  is a parameter that has dimensions of velocity. The Hamiltonian has  $d \equiv 2s+1$  eigenvalues:  $\epsilon_{\mathbf{k}}/(\hbar\vartheta) = \{ks, k(s-1), k(s-2), \dots, -ks\}$ . When  $s$  is an integer, we obtain a dispersionless flat band ( $\epsilon_{\mathbf{k}} = 0$ ), which is absent for half-integer pseudospin. Without any loss of generality, we assume the Fermi energy to have a finite positive value (electron doping).

When  $s \geq 3/2$ , multiple bands cross the Fermi energy, and we need to consider the combined effect from all those bands. We denote the energy dispersion of the bands by  $\epsilon_{\mathbf{k}}^{(ss')} = +\hbar\vartheta s'k$ , where the first label in the superscript ( $ss'$ ) indicates the fermion pseudospin  $s$  and the second label indicates the band with dispersion  $\hbar\vartheta s'k$ .

*Generalized eigenfunctions*

The eigenfunctions corresponding to  $\epsilon_{\mathbf{k}}^{ss'}$  take the following form

$$|\mathbf{k}ss'\rangle = \mathcal{N}_{ss'} \sum_{m=0}^{2s} f_m^{ss'} e^{-im\phi}, \quad (19)$$

where  $\tan \phi = k_y/k_x$ ,  $f_m^{ss'}$  are the coefficients, and  $\mathcal{N}_{ss'}$  is the normalization constant. In later sections, we provide the analytical form of  $f_m^{ss'}$  for a few cases.

*Impurity potential*

We consider  $\delta$ -correlated scalar non-magnetic impurities given by the impurity potential

$$U_0(\mathbf{r}) = \sum_i u_0 \mathbb{I}_{2s+1 \times 2s+1} \delta(\mathbf{r} - \mathbf{R}_i), \quad (20)$$

where the sum is over all impurity sites and  $u_0$  is the impurity strength, assumed to be the same at each site. The scattering (Born) amplitude is

$$U_{\mathbf{k}\mathbf{k}'}^{ss'} = \langle \mathbf{k}ss' | U_0(\mathbf{r}) | \mathbf{k}'ss' \rangle, \quad (21)$$

and the impurity assumes the form

$$\langle U_{\mathbf{k}\mathbf{k}'}^{ss'} U_{\mathbf{k}'\mathbf{k}}^{ss'} \rangle_{\text{imp}} = nu_0^2 \mathcal{F}^{ss'}(\phi - \phi'), \quad (22)$$



where the expression for  $\mathcal{F}^{ss'}(\phi)$  will be provided later. Since the energy dispersion  $\epsilon_{\mathbf{k}}^{ss'}$  depends only on  $s'$ , the density of states also depends only on  $s'$  and is independent of  $s$ :

$$\begin{aligned} N^{ss'}(E) &= \frac{1}{4\pi^2} \int_0^\infty k dk \int_0^{2\pi} d\phi \delta(\epsilon_{\mathbf{k}}^{ss'} - E) \\ &= \frac{1}{2\pi} \int_0^\infty dk k \delta(\epsilon_{\mathbf{k}}^{ss'} - E) \\ &= \frac{E}{2\pi(s'\hbar v)^2} \equiv N^{s'}(E). \end{aligned} \quad (23)$$

The scattering time calculated via the Fermi's Golden rule is

$$\begin{aligned} \frac{1}{\tau_{ss'}} &= \frac{2\pi}{\hbar} \sum_{\mathbf{k}'} \langle U_{\mathbf{k},\mathbf{k}'}^{ss'} U_{\mathbf{k}',\mathbf{k}}^{ss'} \rangle_{\text{imp}} \delta(E_F - \epsilon_{\mathbf{k}'}) \\ &= \frac{2\pi}{\hbar} N_F^{s'} \int_0^{2\pi} \frac{d\phi'}{2\pi} \langle U_{\mathbf{k}\mathbf{k}'}^{ss'} U_{\mathbf{k}'\mathbf{k}}^{ss'} \rangle_{\text{imp}} \\ &= \frac{2\pi}{\hbar} N_F^{s'} \mathcal{G}_{ss'} n_0 u_0^2, \end{aligned} \quad (24)$$

where  $N_F^{s'} = E_F/2\pi(s'\hbar v)^2$  is the density of states at the Fermi energy. The coefficient  $\mathcal{G}_{ss'}$ , which is obtained by the angular integration of  $\langle U_{\mathbf{k}\mathbf{k}'}^{ss'} U_{\mathbf{k}'\mathbf{k}}^{ss'} \rangle_{\text{imp}}$  will be specified later.

### Velocity correction

Next, we evaluate the ladder diagram correction to the velocity. The corresponding equation is given by

$$\tilde{\mathbf{v}}_{\mathbf{k}}^{ss'} = \mathbf{v}_{\mathbf{k}}^{ss'} + \sum_{\mathbf{k}'} G_{\mathbf{k}'}^{ss'R} G_{\mathbf{k}'}^{ss'A} \langle U_{\mathbf{k}\mathbf{k}'}^{ss'} U_{\mathbf{k}'\mathbf{k}}^{ss'} \rangle_{\text{imp}} \tilde{\mathbf{v}}_{\mathbf{k}'}^{ss'}, \quad (25)$$

Here  $G_{\mathbf{k}'}^{ss'R}$  and  $G_{\mathbf{k}'}^{ss'A}$  are retarded and advanced Green's functions respectively, given by

$$G_{\mathbf{k}}^{ss'R/A}(\omega) = \frac{1}{\omega - \epsilon_{\mathbf{k}}^{ss'} \pm \frac{i\hbar}{2\tau_{ss'}}} \quad (26)$$

The ansatz  $\tilde{\mathbf{v}}_{\mathbf{k}}^{ss'} = \eta^{ss'} \mathbf{v}_{\mathbf{k}}^{ss'}$  is substituted in Eq. 25 to obtain the following solution for  $\eta^{ss'}$ :

$$\eta_{ss'} = \frac{\mathcal{G}_{ss'}}{\mathcal{G}_{ss'} - \mathcal{H}_{ss'}}, \quad (27)$$

where

$$\mathcal{G}_{ss'} = \int_0^{2\pi} \frac{d\phi'}{2\pi} \langle U_{\mathbf{k}\mathbf{k}'}^{ss'} U_{\mathbf{k}'\mathbf{k}}^{ss'} \rangle_{\text{imp}}, \text{ and } \mathcal{H}_{ss'} \cos \phi = \int_0^{2\pi} \frac{d\phi'}{2\pi} \cos \phi' \langle U_{\mathbf{k}\mathbf{k}'}^{ss'} U_{\mathbf{k}'\mathbf{k}}^{ss'} \rangle_{\text{imp}}. \quad (28)$$

*Conductivity*

The quantum interference correction to conductivity is obtained by the calculation of a bare Hikami box and two dressed Hikami boxes. The bare Hikami box at zero temperature is calculated as

$$\sigma_0^F = \frac{e^2 \hbar}{2\pi} \sum_{\mathbf{q}} \Gamma(\mathbf{q}) \sum_{\mathbf{k}} \tilde{v}_{\mathbf{k}}^{ss'x} \tilde{v}_{\mathbf{q}-\mathbf{k}}^{ss'x} G_{\mathbf{k}}^{ss'R} G_{\mathbf{k}}^{ss'A} G_{\mathbf{q}-\mathbf{k}}^{ss'R} G_{\mathbf{q}-\mathbf{k}}^{ss'A}, \quad (29)$$

In the small  $\mathbf{q}$  limit, we find

$$\sigma_0^F = -\frac{e^2 s'^2 \vartheta^2 N_F^{s'} \eta_{ss'}^2 \tau_{ss'}^3}{\hbar^2} \sum_{\mathbf{q}} \Gamma(\mathbf{q}) \quad (30)$$

Here  $\Gamma(\mathbf{q})$  is the vertex function which depends on  $\mathbf{q}$  (incoming momentum) and must not be confused with the Gamma function  $\Gamma(d)$ .

Two dressed Hikami boxes denoted as  $\sigma_R^F$  and  $\sigma_A^F$

$$\sigma_R^F = \frac{e^2 \hbar}{2\pi} \sum_{\mathbf{q}} \Gamma(\mathbf{q}) \sum_{\mathbf{k}} \sum_{\mathbf{k}_1} \tilde{v}_{\mathbf{k}}^{ssx} \tilde{v}_{\mathbf{q}-\mathbf{k}_1}^{ssx} G_{\mathbf{k}}^{ssR} G_{\mathbf{k}_1}^{ssR} G_{\mathbf{q}-\mathbf{k}}^{ssR} G_{\mathbf{q}-\mathbf{k}_1}^{ssR} G_{\mathbf{k}}^{ssA} G_{\mathbf{q}-\mathbf{k}_1}^{ssA} \langle U_{\mathbf{k}_1, \mathbf{k}}^{ss} U_{\mathbf{q}-\mathbf{k}_1, \mathbf{q}-\mathbf{k}}^{ss} \rangle_{\text{imp}}, \quad (31)$$

$$\sigma_A^F = \frac{e^2 \hbar}{2\pi} \sum_{\mathbf{q}} \Gamma(\mathbf{q}) \sum_{\mathbf{k}} \sum_{\mathbf{k}_1} \tilde{v}_{\mathbf{k}}^{ssx} \tilde{v}_{\mathbf{q}-\mathbf{k}_1}^{ssx} G_{\mathbf{k}}^{ssR} G_{\mathbf{q}-\mathbf{k}_1}^{ssR} G_{\mathbf{k}}^{ssA} G_{\mathbf{k}_1}^{ssA} G_{\mathbf{q}-\mathbf{k}}^{ssA} G_{\mathbf{q}-\mathbf{k}_1}^{ssA} \langle U_{\mathbf{k}, \mathbf{k}_1}^{ss} U_{\mathbf{q}-\mathbf{k}, \mathbf{q}-\mathbf{k}_1}^{ss} \rangle_{\text{imp}}, \quad (32)$$

We evaluate

$$\sigma_A^F = \sigma_R^F = \frac{e^2 N_F^{s'} \tau_{ss'}^3 \eta_{ss'}^2 \vartheta^2 s'^2}{4\hbar^2 \mathcal{G}_{ss'}} \mathcal{A}_1^{ss'} \sum_{\mathbf{q}} \Gamma(\mathbf{q}) \quad (33)$$

The ratio of dressed to bare Hikami box is given by

$$\frac{\sigma_A^F}{\sigma_0^F} = -\frac{\mathcal{A}_1^{ss'}}{4\mathcal{G}_{ss'}}. \quad (34)$$

The total conductivity is given by the sum of the bare and two dressed Hikami boxes:

$$\sigma^F = -\frac{e^2 N_F^{s'} \tau_{ss'}^3 \eta_{ss'}^2 \vartheta^2 s'^2}{4\hbar^2 \mathcal{G}_{ss'}} \left( 1 - \left( \frac{\mathcal{A}_1^{ss'}}{2\mathcal{G}_{ss'}} \right) \right) \sum_{\mathbf{q}} \Gamma(\mathbf{q}) \quad (35)$$

*Bethe-Salpeter equation*

The Bethe-Salpeter equation for the vertex is given by

$$\mathbf{\Gamma}_{\mathbf{k}_1, \mathbf{k}_2}^{ss'} = \mathbf{\Gamma}_{\mathbf{k}_1, \mathbf{k}_2}^{ss'0} + \sum_{\mathbf{k}} \mathbf{\Gamma}_{\mathbf{k}_1, \mathbf{k}}^{ss'0} G_{\mathbf{k}}^{ss'R} G_{\mathbf{q}-\mathbf{k}}^{ss'A} \mathbf{\Gamma}_{\mathbf{k}, \mathbf{k}_2}^{ss'}, \quad (36)$$

where the bare vertex  $\mathbf{\Gamma}_{\mathbf{k}_1, \mathbf{k}_2}^{ss'0} = \langle U_{\mathbf{k}_1 \mathbf{k}_2}^{ss'} U_{-\mathbf{k}_1 \mathbf{k}_2}^{ss'} \rangle_{\text{imp}}$  takes the following form

$$\mathbf{\Gamma}_{\mathbf{k}_1, \mathbf{k}_2}^{ss'0} = \left( \frac{\hbar}{2\pi N_F^{s'} \mathcal{G}_{ss'} \tau_{ss'}} \right) \sum_{m=0}^{4s} \mathcal{A}_m^{ss'} e^{im(\phi_1 - \phi_2)}, \quad (37)$$



We assume the following ansatz for the vertex:

$$\mathbf{\Gamma}_{\mathbf{k}_1, \mathbf{k}_2}^{ss'} = \left( \frac{\hbar}{2\pi N_F \mathcal{G}_{ss'} \tau_{ss'}} \right) \sum_{m=0}^{4s} \sum_{n=0}^{4s} \mathcal{V}_{mn}^{ss'} e^{i(m\phi_1 - n\phi_2)}, \quad (38)$$

which solves the Bethe-Salpeter equation. The coefficients of the matrix  $\mathcal{V}^{ss'}$  are given by the solution of the following equation:

$$\mathcal{V}^{ss'} = (1 - \mathcal{A}^{ss'} \Phi^{ss'} \mathcal{G}_{ss'}^{-1})^{-1} \mathcal{A}^{ss'}, \quad (39)$$

where

$$\begin{aligned} \Phi_{mn}^{ss'} &= \int \frac{d\phi}{2\pi} \frac{e^{i(n-m)\phi}}{1 + i\tau_{ss'} \vartheta s' q \cos \phi} \\ &= \left(1 - \frac{Q^2}{2}\right) \delta_{mn} - \frac{iQ}{2} (\delta_{m, n+1} + \delta_{m, n-1}) \\ &\quad - \frac{Q^2}{4} (\delta_{m, n+2} + \delta_{m, n-2}), \end{aligned} \quad (40)$$

and  $Q = \vartheta \tau_{ss'} s' q$ . It is possible to express the diagonal elements of the matrix  $\mathcal{V}^{ss'}$  as

$$\mathcal{V}_{ii}^{ss'} = \frac{\mathcal{U}_{ii}^{ss'}}{\mathcal{W}_{ii}^{ss'}}, \quad (41)$$

where

$$\begin{aligned} \mathcal{U}_{ii}^{ss'} &= \mathcal{G}_{ss'} \\ \mathcal{W}_{ii}^{ss'} &= \left(-1 + \frac{\mathcal{G}_{ss'}}{\mathcal{A}_i^{ss'}}\right) + \left(2 \sum_j \frac{\mathcal{A}_j^{ss'}}{\mathcal{G}_{ss'}} + \sum_{j < k} \alpha_{ss'jk}^{(2)} \frac{\mathcal{A}_j^{ss'}}{\mathcal{G}_{ss'}} \frac{\mathcal{A}_k^{ss'}}{\mathcal{G}_{ss'}} \right. \\ &\quad \left. + \sum_{j < k < l} \alpha_{ss'jkl}^{(3)} \frac{\mathcal{A}_j^{ss'}}{\mathcal{G}_{ss'}} \frac{\mathcal{A}_k^{ss'}}{\mathcal{G}_{ss'}} \frac{\mathcal{A}_l^{ss'}}{\mathcal{G}_{ss'}} + \sum_{j < k < l < m} \alpha_{ss'jklm}^{(4)} \frac{\mathcal{A}_j^{ss'}}{\mathcal{G}_{ss'}} \frac{\mathcal{A}_k^{ss'}}{\mathcal{G}_{ss'}} \frac{\mathcal{A}_l^{ss'}}{\mathcal{G}_{ss'}} \frac{\mathcal{A}_m^{ss'}}{\mathcal{G}_{ss'}} + \dots + \beta_{ss'} \prod_j \frac{\mathcal{A}_j^{ss'}}{\mathcal{G}_{ss'}}\right) \frac{Q^2}{D_{ss'}}, \end{aligned} \quad (42)$$

where

$$D_{ss'} = \prod_j \left(-1 + \frac{\mathcal{G}_{ss'}}{\mathcal{A}_j^{ss'}}\right), \quad (43)$$

and the coefficients  $\alpha$  and  $\beta$  can be determined for specific cases. It is of interest to find the Cooperon gaps ( $g_\alpha^{ss'} \equiv 2(-1 + \mathcal{G}_{ss'}/\mathcal{A}_\alpha^{ss'})$ ). Vanishing Cooperon gaps result in diverging elements  $\mathcal{V}_{\alpha\alpha}^{ss'}$  in the limit  $q \rightarrow 0$ .

m 2s+1	0	1	2	3	4	5	6	7	8	9	...
1	1										
2	1	1									
3	1	$\sqrt{2}$	1								
4	1	$\sqrt{3}$	$\sqrt{3}$	1							
5	1	$\sqrt{4}$	$\sqrt{6}$	$\sqrt{4}$	1						
6	1	$\sqrt{5}$	$\sqrt{10}$	$\sqrt{10}$	$\sqrt{5}$	1					
7	1	$\sqrt{6}$	$\sqrt{15}$	$\sqrt{20}$	$\sqrt{15}$	$\sqrt{6}$	1				
8	1	$\sqrt{7}$	$\sqrt{21}$	$\sqrt{35}$	$\sqrt{35}$	$\sqrt{21}$	$\sqrt{7}$	1			
9	1	$\sqrt{8}$	$\sqrt{28}$	$\sqrt{56}$	$\sqrt{70}$	$\sqrt{56}$	$\sqrt{28}$	$\sqrt{8}$	1		
10	1	$\sqrt{9}$	$\sqrt{36}$	$\sqrt{84}$	$\sqrt{126}$	$\sqrt{126}$	$\sqrt{84}$	$\sqrt{36}$	$\sqrt{9}$	1	...
...	...	...	...	...	...	...	...	...	...	...	...

Figure 5. Wavefunction coefficients  $f_m^{ss}$  have the mathematical structure of square-root of the Pascal's triangle.

### The case $s = s'$

Our focus here is the topmost conduction band with energy dispersion  $\epsilon_{\mathbf{k}} = \hbar\partial sk$ . In this case, it is possible to analytically find out the various coefficients introduced earlier.

$$\begin{aligned}
f_m^{ss} &= \left( \frac{\Gamma(2s+1)}{\Gamma(m+1)\Gamma(2s+1-m)} \right)^{1/2} \\
\mathcal{N}_{ss} &= \frac{1}{\sqrt{2^{2s}}} \\
\mathcal{F}^{ss}(\phi) &= \cos^{4s}(\phi/2) \\
\mathcal{G}_{ss} &= \frac{\Gamma(2s+1/2)}{\sqrt{\pi}\Gamma(2s+1)} \\
\mathcal{H}_{ss} &= \frac{\Gamma(2s+1/2)}{\sqrt{\pi}(\Gamma(2s)+2s\Gamma(2s))} \\
\eta^{ss} &= 2s+1 \\
\mathcal{A}_{0 \leq m \leq 2s}^{ss} &= \frac{\Gamma(2s+1/2)}{\sqrt{\pi} \left( \prod_{k=0}^{k=2s-m-1} 4s-m-k \right) m!} \\
\mathcal{A}_{2s \leq m \leq 4s}^{ss} &= \mathcal{A}_{4s-m}^{ss},
\end{aligned} \tag{44}$$

where  $\Gamma(x)$  is the Gamma-function. Remarkably, the wavefunction coefficients  $f_m^{ss}$  have the mathematical structure of square-root of the Pascal's triangle as shown in Fig. 5.

Furthermore, the following condition guarantees that the Cooperon gap vanishes:

$$g_{\alpha}^{ss} = \frac{\mathcal{G}_{ss}}{\mathcal{A}_{\alpha}^{ss}} = 1. \tag{45}$$

The above condition is satisfied for  $\alpha = 2s$ . Therefore in the limit  $q \rightarrow 0$ , the vertex correction is dominated by the following term:

$$\mathbf{\Gamma}_{\mathbf{k}_1 \mathbf{k}_2}^{ss'} \sim \frac{1}{q^2} e^{2is(\phi_1 - \phi_2)}. \tag{46}$$

When  $\phi_1 - \phi_2 \approx \pi$ , the vertex carries a positive (negative) sign for integer (half-integer) values of  $s$ . This implies weak-localization for integer  $s$  and weak-antilocalization for half-integer  $s$ .

Furthermore, we recover the known results for graphene:

$$\begin{aligned}\eta^{\frac{1}{2}\frac{1}{2}} &= 2 \\ \mathcal{F}^{\frac{1}{2}\frac{1}{2}}(\phi) &= \cos^2(\phi/2) \\ \frac{\sigma_A^F}{\sigma_0^F} &= -\frac{\mathcal{A}_1^{\frac{1}{2}\frac{1}{2}}}{4\mathcal{G}_{\frac{1}{2}\frac{1}{2}}} = -\frac{1}{4}.\end{aligned}\tag{47}$$

### The case $s' \neq s$

When  $s' \neq s$ , finding generalized analytical expressions is a cumbersome task. We explicitly evaluate the coefficients for the first few cases ( $s \leq 7/2$ ). Table I, II, III, IV and present the values of the coefficients  $\mathcal{G}^{ss'}$  and  $\mathcal{H}^{ss'}$ , respectively. The velocity correction coefficients is presented in Table V and VI. Interestingly, we find that the flat bands in the even  $s$  case have  $\eta^{ss'} = 0$ , implying zero velocity correction. The bare Cooperon coefficients  $A^{ss'}$  are presented in Table VII and Table VIII for the odd  $s$  and even  $s$  cases, respectively. We find that the value  $\alpha$  for which the Cooperon gap  $g_\alpha^{ss'}$  vanishes is independent of  $s'$ . Therefore, when multiple bands cross the Fermi energy (for  $s \geq 3/2$ ), each band results in the same qualitative behavior, i.e., localization for even  $s$  and antilocalization for odd  $s$ .

### Conductivity

The zero-field conductivity from  $|\mathbf{k}ss'\rangle$  is finally evaluated to be

$$\sigma_{ss'} = -\sum_{\alpha} \frac{e^2}{\pi h} Y_{\alpha}^{ss'} \int d(q^2) \frac{1}{l_{ss'\alpha}^{-2} + q^2},\tag{48}$$

where

$$\begin{aligned}Y_{\alpha}^{ss'} &= \frac{\eta^{ss'2} s'^2}{4X_{\alpha}^{ss'} \mathcal{G}^{ss'2}} \left(1 - \frac{A_1^{ss'}}{2\mathcal{G}^{ss'}}\right), \\ l_{ss'\alpha}^{-2} &= \frac{g_{\alpha}^{ss'}}{2X_{\alpha}^{ss'} l_{ss'}^2}, \\ l_{ss'}^2 &= \frac{2}{\vartheta^2 \tau_{ss'}^2}\end{aligned}\tag{49}$$

and the vertex  $\Gamma_{\mathbf{q}}^{ss'}$  is expressed as

$$\Gamma_{\mathbf{q}}^{ss'} = \frac{\hbar}{2\pi N_F^{s'} \tau_{ss'}} \sum_{\alpha} \frac{2}{g_{\alpha}^{ss'2} + X_{\alpha}^{ss'} Q^2} e^{i\alpha\pi}\tag{50}$$

The vanishing Cooperon gaps will result in the most dominant contribution to the conductivity. The values of  $\alpha$  such that  $g_{\alpha}^{ss'} = 0$ , and the corresponding  $X_{\alpha}^{ss'}$  are presented in Table IX. In the weak-field limit, the magnetoconductivity is given by

$$\Delta\sigma(B)_{ss'} = \frac{e^2}{\pi h} \sum_{\alpha} Y_{\alpha}^{ss'} \left[ \Psi \left( \frac{l_B^2}{l_{\phi}^2} + \frac{l_B^2}{l_{ss'\alpha}^2} + \frac{1}{2} \right) - \log \left( \frac{l_B^2}{l_{\phi}^2} + \frac{l_B^2}{l_{ss'\alpha}^2} \right) \right],\tag{51}$$

where  $\Psi(x)$  is the digamma function,  $l_{\phi}$  is the coherence length, and  $l_B = \sqrt{\hbar/4eB}$  is the magnetic length of a Cooperon.

$s' \rightarrow$	$-\frac{7}{2}$	$-\frac{5}{2}$	$-\frac{3}{2}$	$-\frac{1}{2}$	$\frac{1}{2}$	$\frac{3}{2}$	$\frac{5}{2}$	$\frac{7}{2}$
$s \downarrow$								
$\frac{1}{2}$	-	-	-	$\frac{1}{2}$	$\frac{1}{2}$	-	-	-
$\frac{3}{2}$	-	-	$\frac{5}{16}$	$\frac{5}{16}$	$\frac{5}{16}$	$\frac{5}{16}$	-	-
$\frac{5}{2}$	-	$\frac{63}{256}$	$\frac{55}{256}$	$\frac{15}{64}$	$\frac{15}{64}$	$\frac{55}{256}$	$\frac{63}{256}$	-
$\frac{7}{2}$	$\frac{429}{2048}$	$\frac{357}{2048}$	$\frac{349}{2048}$	$\frac{389}{2048}$	$\frac{389}{2048}$	$\frac{349}{2048}$	$\frac{357}{2048}$	$\frac{429}{2048}$

Table I.  $\mathcal{G}^{ss'}$  for odd pseudospin- $s$  fermions.

$s' \rightarrow$	-3	-2	-1	0	1	2	3
$s \downarrow$							
1	-	-	$\frac{3}{8}$	$\frac{1}{2}$	$\frac{3}{8}$	-	-
2	-	$\frac{35}{128}$	$\frac{1}{4}$	$\frac{11}{32}$	$\frac{1}{4}$	$\frac{35}{128}$	-
3	$\frac{231}{1024}$	$\frac{49}{256}$	$\frac{199}{1024}$	$\frac{17}{64}$	$\frac{199}{1024}$	$\frac{49}{256}$	$\frac{231}{1024}$

Table II.  $\mathcal{G}^{ss'}$  for even pseudospin- $s$  fermions.

$s' \rightarrow$	$-\frac{7}{2}$	$-\frac{5}{2}$	$-\frac{3}{2}$	$-\frac{1}{2}$	$\frac{1}{2}$	$\frac{3}{2}$	$\frac{5}{2}$	$\frac{7}{2}$
$s \downarrow$								
$\frac{1}{2}$	-	-	-	$\frac{1}{4}$	$\frac{1}{4}$	-	-	-
$\frac{3}{2}$	-	-	$\frac{15}{64}$	$\frac{7}{64}$	$\frac{7}{64}$	$\frac{15}{64}$	-	-
$\frac{5}{2}$	-	$\frac{105}{512}$	$\frac{65}{512}$	$\frac{9}{128}$	$\frac{9}{128}$	$\frac{65}{512}$	$\frac{105}{512}$	-
$\frac{7}{2}$	$\frac{3003}{16384}$	$\frac{1995}{16384}$	$\frac{1443}{16384}$	$\frac{851}{16384}$	$\frac{851}{16384}$	$\frac{1443}{16384}$	$\frac{1995}{16384}$	$\frac{3003}{16384}$

Table III.  $\mathcal{H}^{ss'}$  for odd pseudospin- $s$  fermions.

$s' \rightarrow$	-3	-2	-1	0	1	2	3
$s \downarrow$							
1	-	-	$\frac{1}{4}$	0	$\frac{1}{4}$	-	-
2	-	$\frac{7}{8}$	$\frac{1}{8}$	0	$\frac{1}{8}$	$\frac{7}{8}$	-
3	$\frac{99}{512}$	$\frac{1}{8}$	$\frac{43}{512}$	0	$\frac{43}{512}$	$\frac{1}{8}$	$\frac{99}{512}$

Table IV.  $\mathcal{H}^{ss'}$  for even pseudospin- $s$  fermions.

$s' \rightarrow$	$-\frac{7}{2}$	$-\frac{5}{2}$	$-\frac{3}{2}$	$-\frac{1}{2}$	$\frac{1}{2}$	$\frac{3}{2}$	$\frac{5}{2}$	$\frac{7}{2}$
$s \downarrow$								
$\frac{1}{2}$	-	-	-	2	2	-	-	-
$\frac{3}{2}$	-	-	4	$\frac{20}{13}$	$\frac{20}{13}$	4	-	-
$\frac{5}{2}$	-	6	$\frac{22}{9}$	$\frac{10}{7}$	$\frac{10}{7}$	$\frac{22}{9}$	8	-
$\frac{7}{2}$	8	$\frac{136}{41}$	$\frac{2792}{1349}$	$\frac{3112}{2261}$	$\frac{3112}{2261}$	$\frac{2792}{1349}$	$\frac{136}{41}$	8

Table V. The velocity correction  $\eta^{ss'}$  for odd pseudospin- $s$  fermions.

$s' \rightarrow$	-3	-2	-1	0	1	2	3
$s \downarrow$							
1	-	-	3	1	3	-	-
2	-	5	2	1	2	5	-
3	7	$\frac{49}{17}$	$\frac{199}{113}$	1	$\frac{199}{113}$	$\frac{49}{17}$	7

Table VI. The velocity correction  $\eta^{ss'}$  for even pseudospin- $s$  fermions.

$s$	$s'$	$\mathcal{A}_0^{ss'}$	$\mathcal{A}_1^{ss'}$	$\mathcal{A}_2^{ss'}$	$\mathcal{A}_3^{ss'}$	$\mathcal{A}_4^{ss'}$	$\mathcal{A}_5^{ss'}$	$\mathcal{A}_6^{ss'}$	$\mathcal{A}_7^{ss'}$	$\mathcal{A}_8$	$\mathcal{A}_9^{ss'}$	$\mathcal{A}_{10}^{ss'}$
$\frac{1}{2}$	$\frac{1}{2}$	$\frac{1}{4}$	$\frac{1}{2}$	$\frac{1}{4}$								
$\frac{1}{2}$	$-\frac{1}{2}$	$\frac{1}{4}$	$\frac{1}{2}$	$\frac{1}{4}$								
$\frac{3}{2}$	$\frac{3}{2}$	$\frac{1}{64}$	$\frac{3}{32}$	$\frac{15}{64}$	$\frac{5}{16}$	$\frac{15}{64}$	$\frac{3}{32}$	$\frac{1}{64}$				
$\frac{3}{2}$	$\frac{1}{2}$	$\frac{9}{64}$	$\frac{3}{32}$	$\frac{7}{64}$	$\frac{5}{16}$	$\frac{15}{64}$	$\frac{3}{32}$	$\frac{1}{64}$				
$\frac{3}{2}$	$-\frac{1}{2}$	$\frac{9}{64}$	$\frac{3}{32}$	$\frac{7}{64}$	$\frac{5}{16}$	$\frac{7}{64}$	$\frac{3}{32}$	$\frac{9}{64}$				
$\frac{3}{2}$	$-\frac{3}{2}$	$\frac{1}{64}$	$\frac{3}{32}$	$\frac{15}{64}$	$\frac{5}{16}$	$\frac{15}{64}$	$\frac{3}{32}$	$\frac{1}{64}$				
$\frac{5}{2}$	$\frac{5}{2}$	$\frac{1}{1024}$	$\frac{5}{512}$	$\frac{45}{1024}$	$\frac{15}{128}$	$\frac{105}{512}$	$\frac{63}{256}$	$\frac{105}{512}$	$\frac{15}{128}$	$\frac{45}{1024}$	$\frac{5}{512}$	$\frac{1}{1024}$
$\frac{5}{2}$	$\frac{3}{2}$	$\frac{25}{1024}$	$\frac{45}{512}$	$\frac{101}{1024}$	$\frac{7}{128}$	$\frac{65}{512}$	$\frac{55}{256}$	$\frac{65}{512}$	$\frac{7}{128}$	$\frac{101}{1024}$	$\frac{45}{512}$	$\frac{25}{1024}$
$\frac{5}{2}$	$\frac{1}{2}$	$\frac{25}{256}$	$\frac{5}{128}$	$\frac{21}{256}$	$\frac{3}{32}$	$\frac{9}{128}$	$\frac{15}{64}$	$\frac{9}{128}$	$\frac{3}{32}$	$\frac{21}{256}$	$\frac{5}{128}$	$\frac{25}{256}$
$\frac{5}{2}$	$-\frac{1}{2}$	$\frac{25}{256}$	$\frac{5}{128}$	$\frac{21}{256}$	$\frac{3}{32}$	$\frac{9}{128}$	$\frac{15}{64}$	$\frac{9}{128}$	$\frac{3}{32}$	$\frac{21}{256}$	$\frac{5}{128}$	$\frac{25}{256}$
$\frac{5}{2}$	$-\frac{3}{2}$	$\frac{25}{1024}$	$\frac{45}{512}$	$\frac{101}{1024}$	$\frac{7}{128}$	$\frac{65}{512}$	$\frac{55}{256}$	$\frac{65}{512}$	$\frac{7}{128}$	$\frac{101}{1024}$	$\frac{45}{512}$	$\frac{25}{1024}$
$\frac{5}{2}$	$-\frac{5}{2}$	$\frac{1}{1024}$	$\frac{5}{512}$	$\frac{45}{1024}$	$\frac{15}{128}$	$\frac{105}{512}$	$\frac{63}{256}$	$\frac{105}{512}$	$\frac{15}{128}$	$\frac{45}{1024}$	$\frac{5}{512}$	$\frac{1}{1024}$

Table VII. Bare Cooperon coefficients  $\mathcal{A}^{ss'}$  for odd pseudospin- $s$  fermions. The highlighted blue color indicates  $\mathcal{A}_\alpha^{ss'} = \mathcal{G}_{ss'}$ , which is the condition for vanishing Cooperon gap  $g_\alpha$ .

		$\mathcal{A}_0^{ss'}$	$\mathcal{A}_1^{ss'}$	$\mathcal{A}_2^{ss'}$	$\mathcal{A}_3^{ss'}$	$\mathcal{A}_4^{ss'}$	$\mathcal{A}_5^{ss'}$	$\mathcal{A}_6^{ss'}$	$\mathcal{A}_7^{ss'}$	$\mathcal{A}_8^{ss'}$	$\mathcal{A}_9^{ss'}$	$\mathcal{A}_{10}^{ss'}$	$\mathcal{A}_{11}^{ss'}$	$\mathcal{A}_{12}^{ss'}$
$s$	$s'$													
1	1	$\frac{1}{16}$	$\frac{1}{4}$	$\frac{3}{8}$	$\frac{1}{4}$	$\frac{1}{16}$								
1	0	$\frac{1}{4}$	0	$\frac{1}{2}$	0	$\frac{1}{4}$								
1	-1	$\frac{1}{16}$	$\frac{1}{4}$	$\frac{3}{8}$	$\frac{1}{4}$	$\frac{1}{16}$								
2	2	$\frac{1}{256}$	$\frac{1}{32}$	$\frac{7}{64}$	$\frac{7}{32}$	$\frac{35}{128}$	$\frac{7}{32}$	$\frac{7}{64}$	$\frac{1}{32}$	$\frac{1}{256}$				
2	1	$\frac{1}{16}$	$\frac{1}{8}$	$\frac{1}{16}$	$\frac{1}{8}$	$\frac{1}{4}$	$\frac{1}{8}$	$\frac{1}{16}$	$\frac{1}{8}$	$\frac{1}{16}$				
2	0	$\frac{9}{64}$	0	$\frac{3}{16}$	0	$\frac{11}{32}$	0	$\frac{3}{16}$	0	$\frac{9}{64}$				
2	-1	$\frac{1}{16}$	$\frac{1}{8}$	$\frac{1}{16}$	$\frac{1}{8}$	$\frac{1}{4}$	$\frac{1}{8}$	$\frac{1}{16}$	$\frac{1}{8}$	$\frac{1}{16}$				
2	-2	$\frac{1}{256}$	$\frac{1}{32}$	$\frac{7}{64}$	$\frac{7}{32}$	$\frac{35}{128}$	$\frac{7}{32}$	$\frac{7}{64}$	$\frac{1}{32}$	$\frac{1}{256}$				
3	3	$\frac{1}{4096}$	$\frac{3}{1024}$	$\frac{33}{2048}$	$\frac{55}{1024}$	$\frac{495}{4096}$	$\frac{99}{512}$	$\frac{231}{1024}$	$\frac{99}{512}$	$\frac{495}{4096}$	$\frac{55}{1024}$	$\frac{33}{2048}$	$\frac{3}{1024}$	$\frac{1}{4096}$
3	2	$\frac{9}{1024}$	$\frac{3}{64}$	$\frac{47}{512}$	$\frac{5}{64}$	$\frac{55}{1024}$	$\frac{1}{8}$	$\frac{49}{256}$	$\frac{1}{8}$	$\frac{55}{1024}$	$\frac{5}{64}$	$\frac{47}{512}$	$\frac{3}{64}$	$\frac{9}{1024}$
3	1	$\frac{225}{4096}$	$\frac{75}{1024}$	$\frac{65}{2048}$	$\frac{95}{1024}$	$\frac{271}{4096}$	$\frac{43}{512}$	$\frac{199}{1024}$	$\frac{43}{512}$	$\frac{271}{4096}$	$\frac{95}{1024}$	$\frac{65}{2048}$	$\frac{75}{1024}$	$\frac{225}{4096}$
3	0	$\frac{25}{256}$	0	$\frac{15}{128}$	0	$\frac{39}{256}$	0	$\frac{17}{64}$	0	$\frac{39}{256}$	0	$\frac{15}{128}$	0	$\frac{25}{256}$
3	-1	$\frac{225}{4096}$	$\frac{75}{1024}$	$\frac{65}{2048}$	$\frac{95}{1024}$	$\frac{271}{4096}$	$\frac{43}{512}$	$\frac{199}{1024}$	$\frac{43}{512}$	$\frac{271}{4096}$	$\frac{95}{1024}$	$\frac{65}{2048}$	$\frac{75}{1024}$	$\frac{225}{4096}$
3	-2	$\frac{9}{1024}$	$\frac{3}{64}$	$\frac{47}{512}$	$\frac{5}{64}$	$\frac{55}{1024}$	$\frac{1}{8}$	$\frac{49}{256}$	$\frac{1}{8}$	$\frac{55}{1024}$	$\frac{5}{64}$	$\frac{47}{512}$	$\frac{3}{64}$	$\frac{9}{1024}$
3	-3	$\frac{1}{4096}$	$\frac{3}{1024}$	$\frac{33}{2048}$	$\frac{55}{1024}$	$\frac{495}{4096}$	$\frac{99}{512}$	$\frac{231}{1024}$	$\frac{99}{512}$	$\frac{495}{4096}$	$\frac{55}{1024}$	$\frac{33}{2048}$	$\frac{3}{1024}$	$\frac{1}{4096}$

Table VIII. Bare Cooperon coefficients  $\mathcal{A}^{ss'}$  for even pseudospin- $s$  fermions. The highlighted blue color indicates  $\mathcal{A}_\alpha^{ss'} = \mathcal{G}_{ss'}$ , which is the condition for vanishing Cooperon gap  $g_\alpha$ .

		$\alpha$	$X_\alpha^{ss'}$
$s$	$s'$		
1/2	1/2	1	1
1/2	-1/2	1	1
1	1	2	1/2
1	0	2	1
1	-1	2	1/2
3/2	3/2	3	5/16
3/2	1/2	3	13/16
3/2	-1/2	3	13/16
3/2	-3/2	3	5/16
2	2	4	7/32
2	1	4	1/2
2	0	4	5/8
2	-1	4	1/2
2	-2	4	7/32
5/2	5/2	5	21/128
5/2	3/2	5	45/128
5/2	1/2	5	21/32
5/2	-1/2	5	21/32
5/2	-3/2	5	45/128
5/2	-5/2	5	21/128
3	3	6	33/256
3	2	6	17/64
3	1	6	113/256
3	0	6	29/64
3	-1	6	113/256
3	-2	6	17/64
3	-3	6	33/256

Table IX. The values  $\alpha$  such that  $g_\alpha^{ss'} = 0$ , and the corresponding  $X_\alpha^{ss'}$